SmO thin films: A flexible route to correlated flat bands with nontrivial topology

Deepa Kasinathan,[1] Klaus Koepernik,[2] L. H. Tjeng,[1] and Maurits W. Haverkort[1]
[1]*Max-Planck-Institut für Chemische Physik fester Stoffe, Nöthnitzer Strasse 40, 01187 Dresden, Germany*
[2]*IFW Dresden, P.O. Box 270116, D-01171 Dresden, Germany*
(Received 24 September 2014; revised manuscript received 3 May 2015; published 18 May 2015)

Using density functional theory based calculations, we show that the correlated mixed-valent compound SmO is a three-dimensional strongly topological semimetal as a result of a $4f$-$5d$ band inversion at the X point. The [001] surface Bloch spectral density reveals two weakly interacting Dirac cones that are quasidegenerate at the $\bar{M}$ point and another single Dirac cone at the $\bar{\Gamma}$ point. We also show that the topological nontriviality in SmO is very robust and prevails for a wide range of lattice parameters, making it an ideal candidate to investigate topological nontrivial correlated flat bands in thin-film form. Moreover, the electron filling is tunable by strain. In addition, we find conditions for which the inversion is of the $4f$-$6s$ type, making SmO to be a rather unique system. The similarities of the crystal symmetry and the lattice constant of SmO to the well studied ferromagnetic semiconductor EuO, makes SmO/EuO thin film interfaces an excellent contender towards realizing the quantum anomalous Hall effect in a strongly correlated electron system.

DOI: 10.1103/PhysRevB.91.195127 PACS number(s): 71.27.+a, 03.65.Vf, 73.20.At, 74.20.Pq

I. INTRODUCTION

Topological insulators (TIs) are materials which exhibit a fundamentally new physical phenomena that was first predicted by theorists [1–7] and subsequently ascertained in experiments [8–12]. Although most work considers band semiconductors, the concept of topology can be extended to correlated systems for which many exciting new effects can be expected. In analogy to correlation driven fractional quantum Hall states one might expect fractional Chern insulating states to emerge in correlated topological insulators [13–17]. The experimental realization of such states would open a whole new field of possibilities.

SmB_6 was recently reported to be a correlated mixed valent topological insulator [18–23]. The highly correlated flat Sm-f derived bands hybridize with the dispersive and itinerant Sm-d derived bands to form a mixed valent insulating ground state. Although the insulating state and topology of the bulk of SmB_6 is well defined, [001] surface of SmB_6 is polar and therefore inherently unstable [24]. This hinders the unique determination of topological surface states and in turn inhibits the creation of robust technological devices. Here, using density functional theory (DFT) based calculations, we show that SmO is a mixed valent correlated compound with a band structure similar to the topological nontrivial high-pressure gold phase of SmS [25]. In contrast to SmS, SmO is predicted to have a topological nontrivial ground state at ambient pressure. Additionally, our calculations show that the topological nontrivial ground state of SmO is stable for a large range of Sm-O distances, including both positive and negative strain. The Sm-f band filling is thus tunable by strain, which opens up the possibility to create correlated topological nontrivial bands at different filling. Subsequent to the enormous success in the design and fabrication of semiconductors, it is presently possible to grow high-quality oxide thin films and heterostructures [26,27]. SmO thus seems the ideal candidate for the experimental realization of topological nontrivial correlated flat bands. In addition, experimental realization of the theoretically predicted quantum anomalous Hall effect (QAHE) (quantized Hall conductance in the absence of an external magnetic field) has been challenging due to difficulties in obtaining insulating bulk TIs concurrent with homogeneous magnetic doping [28]. Recently, notwithstanding the presence of bulk carrier density (i.e., not a nominally insulating bulk), long range ferromagnetism and QAHE was successfully observed in Cr-doped $(Bi,Sb)_2Te_3$ TI thin films [29,30]. Other proposals towards realizing a QAHE are to either grow a TI on top of a ferromagnetic insulator [31,32], transition-metal oxide heterostructures [33,34], or to deposit a layer of heavy atoms with large spin-orbit coupling on a magnetic insulator [35]. Fortuitously, a well studied substrate with the same symmetry as SmO is readily available in the form of the ferromagnetic semiconductor EuO [36–42]. Consequently, we propose growing SmO/EuO thin film interfaces to test the feasibility of obtaining a QAHE in a strongly correlated electron system.

SmO crystallizes in the rock-salt structure with $a =$ 4.9414–4.943 Å [43,44]. Considering the lattice parameters of trivalent neodymium chalcogenides and interpolating between neodymium and terbium compounds, Leger *et al.* obtain a lattice constant of 4.917 Å for $Sm^{3+}O$ [43]. Similarly, considering other divalent lanthanide oxides, a lattice constant of 5.15 Å is expected for $Sm^{2+}O$. Ergo, the experimental cell parameter of fcc SmO lies between that of $Sm^{3+}O$ and $Sm^{2+}O$, which lead the authors [43] to conclude that samarium is in an intermediate valence state in SmO. Using Vegard's law, a valence of 2.92 was assigned [43]. Electrical resistivity measurements as a function of temperature reveals a T^2 like increase between 4.2 and 20 K, followed by a rapid increase up to 32 K. The resistivity shows a linear temperature dependence above 60 K [45]. Krill and co-workers [44] measured the magnetic susceptibility of SmO and observed the roughly constant magnetic susceptibility and the nondivergence of the low-temperature susceptibility. They drew parallels to the susceptibilities of other intermediate valence compounds SmB_6 and gold-SmS under pressure, wherein the low temperature behavior is not explainable by crystal field effects alone [44].

II. METHODS

The electronic structure calculations are performed using the full-potential nonorthogonal local orbital code

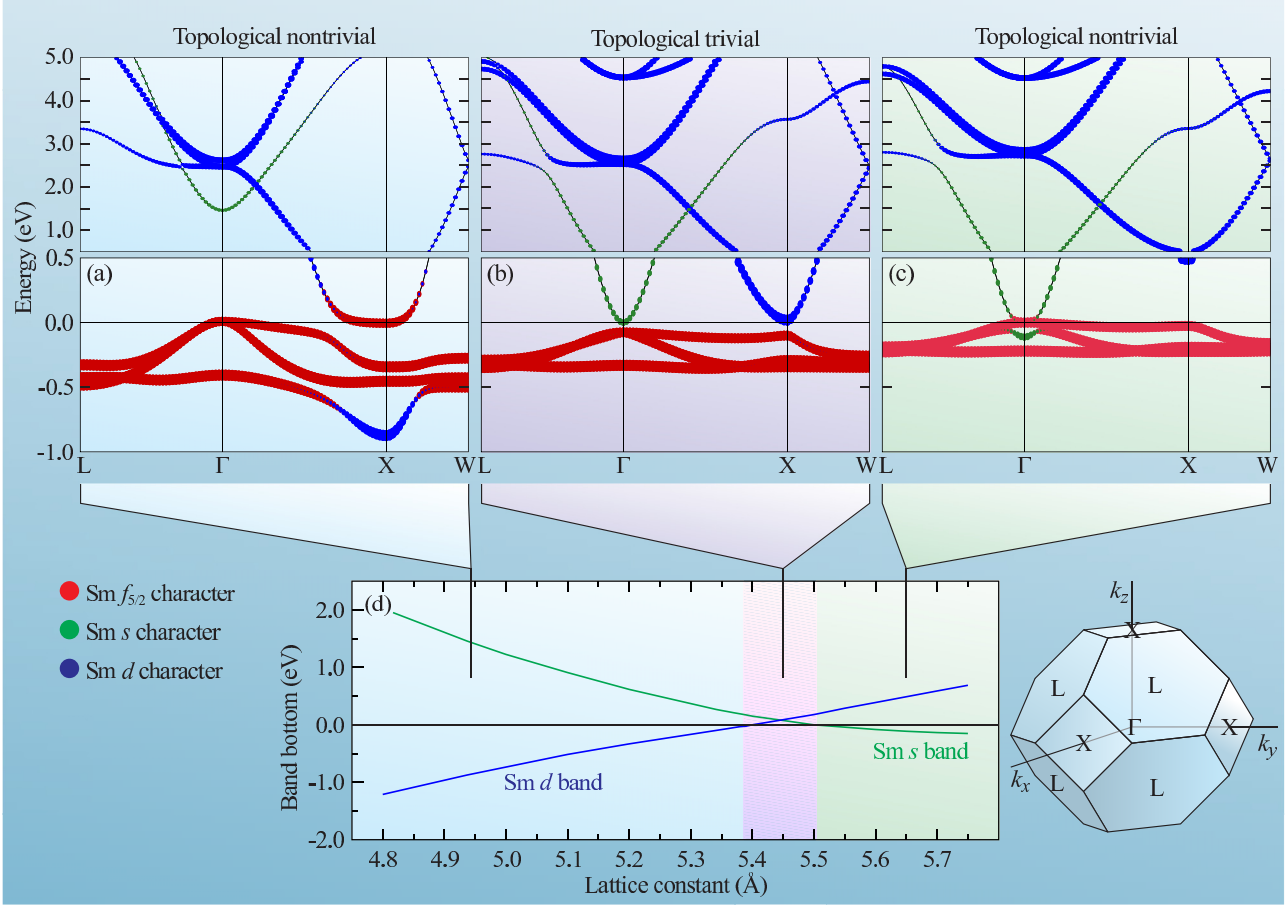

FIG. 1. (Color online) Phase diagram (d) of SmO as a function of the fcc lattice parameter within LDA+SO+U ($U = 6$ eV, $J_H = 0$ eV) along with representative FPLO band structures for the (a) nontrivial d-f band inversion, (b) trivial insulator, and (c) nontrivial s-f band inversion scenarios. The $4f$, $5d$, and $6s$ orbital character derived bands are represented by red, blue, and green colored symbols, respectively. The size of the symbols represent the weight of the various orbital contributions to the underlying bands. The Brillouin zone of an fcc lattice is displayed along with the eight time reversal invariant momenta (TRIM) points.

(FPLO) [46]. The local density approximation (LDA) with the Perdew and Wang flavor [47] of the exchange and correlation potential was chosen. To account for the strong spin-orbit (SO) coupling of the f electrons, we employ the full four-component relativistic scheme. Additionally, the strong Coulomb repulsion between the $4f$ electrons of samarium are included in a mean-field way by applying LDA+SO+U with the "fully localized limit" (FLL) double counting term [48]. This level of theory will not suffice to describe quantitatively the Sm $4f$ spectral weight and its dispersion, but is sufficient to predict the Sm d-f inversion. We have tested the robustness of these predictions by varying U (5 to 7 eV) and J_H (0 to 0.7 eV) and by using different functionals (LDA and GGA using FPLO and the modified Becke-Johnson approach [49] with $U = 3$ eV and $J_H = 0$ eV using Wien2k [50]). Importantly, as pointed out by Martin and Allen [51] for SmB_6 and related systems, the symmetry of the relevant Sm one particle orbitals and the many-body electron removal Green's function is the same. This allows for a possible adiabatic continuation from the LDA results as presented here to the full interacting system without changing the topology of the system. See the Appendix for further discussion on the Sm $4f$ many-body state.

III. RESULTS

Collected in Fig. 1(a) is the FPLO nonspin polarized, full-relativistic band structure of SmO with the inclusion of the strong Coulomb interaction (LDA+SO+U) for the experimental lattice constant. With samarium being in the 2+ configuration, the $4f$ states are split into lower lying and filled $4f_{5/2}$ states that can accommodate six electrons and higher lying (above 5.5 eV), empty $4f_{7/2}$ states (see the Appendix). We do not observe a direct energy gap around the Fermi level (E_F). The material is semimetallic with a "warped gap" such that everywhere in the BZ (at E_F), band number x is always below band number $x + 1$. There are small electron and hole pockets at X and Γ, respectively, but there are no band crossings between the highest occupied $4f_{5/2}$ bands and the lowest unoccupied bands. Besides, varying U (5 to 7 eV) or J_H (0 to 0.7 eV) does not change the above mentioned features, since the oxygen $2p$ and samarium $5d$ and $6s$ bands experience a constant shift with respect to the localized $4f$ states. There exists only one report [45] in literature on the transport properties of SmO wherein the resistivity decreases with decreasing temperature and thus could hint to metallic character, consistent with the lack of an energy gap in our

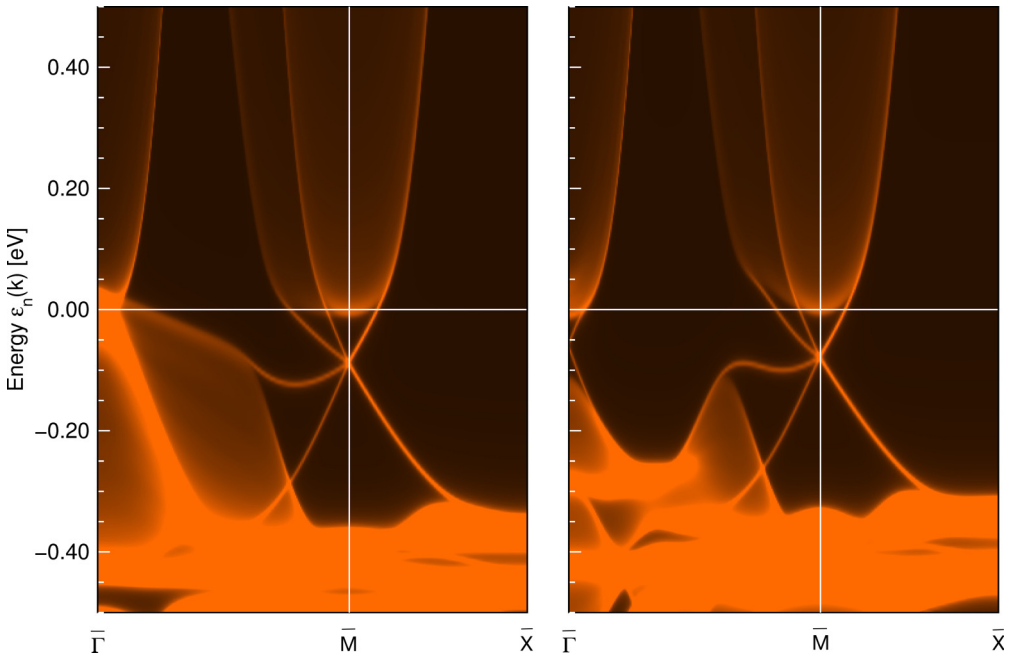

FIG. 2. (Color online) Left: Surface Bloch spectral density $[A_{\mathrm{Bl}}(k)]$ of the first 12 SmO layers of a semi-infinite solid with [001] surface. Note that there are two Dirac cones at the $\bar{X}$ point, while the one at the $\bar{\Gamma}$ point falls into the bulk projected band structure and hence forms a surface resonance (see right panel). Right: $A_{\mathrm{Bl}}(k)$ with a downward shifted $4f$-electron pocket around the $\bar{\Gamma}$ point to reveal the third Dirac cone.

calculations. In contrast to the localized and not very dispersive $4f$ bands, the $5d$ bands of samarium are dispersive, broad, and dip below the Fermi level, retaining a 100% weight at the X point. As a consequence, we observe a $4f$-$5d$ band inversion at the X point, resulting in a nontrivial topology, similar in sense to the band inversions reported for SmB_6 and the high pressure gold phase of SmS. This band inversion and the resulting topological indices 1;(000) allows us to classify SmO as a three-dimensional (3D) strongly topological semimetal (more details are provided in the Appendix).

A well known issue with LDA when dealing with semiconductors, is the underestimation of band gaps. Since nontrivial topology depends on band inversions, underestimation of band gaps could sometimes lead to a wrong sequence of the underlying band structure. For example, in HgTe, a s-p TI, LDA correctly predicts the band inversion, but results in an incorrect band sequence at the Γ point. The correct band sequence is obtained by using the MBJLDA exchange potential [52]. Literature on the efficiency of MBJLDA over the traditional LDA+U for f electron systems is still scarce. In a recent work on SmS, the authors have employed MBJLDA+SO+U ($U = 3$ eV) to open a band gap of 0.2 eV in the ambient pressure black phase such that the gap is consistent with the available experiments [25]. Using the same parameters, the authors conclude that the high pressure gold phase of SmS is a topological metal. We compared the LDA+SO+U results with that of MBJLDA+SO and obtain a consistent picture for the band inversion between the two approaches (see the Appendix). No direct band gap is opened with MBJLDA+SO+U ($U = 3$ eV), in accordance with our LDA+SO+U results and as well as with the experimental report [45].

To provide additional confirmation of the topological nontriviality in SmO and to explicitly identify the protected surface states, we have calculated the Bloch spectral density $[A_{\mathrm{Bl}}(k)]$ of the 12 topmost surface layers of a semi-infinite solid [53] with [001] surface (Fig. 2). We obtain two weakly interacting quasidegenerate Dirac cones at $\bar{M}$, and a single Dirac cone at $\bar{\Gamma}$, which is hidden in the bulk and becomes a surface resonance due to the semimetallic nature of SmO. To clearly identify the Dirac cone at $\bar{\Gamma}$, we have repeated the slab calculations such that the hole pockets at Γ for the bulk are pushed down. This in turn allows one to unambiguously identify all three Dirac cones in a [001] terminated SmO. More details are provided in the Appendix.

Having established the nontrivial topology in SmO for the experimental bulk lattice parameter, we consider the scenario of growing thin films of SmO. In general, the lattice parameter of the substrate plays a decisive role in determining the lattice parameter of the thin film. Then, the relevant question to answer is the robustness of the topological semimetal state as a function of lattice parameter variation. To this end, we have investigated the topological indices for various lattice parameters. We have retained the cubic symmetry of the unit cell (i.e., isotropic volume change) in SmO, based on the experimental studies on isostructural samarium systems, which evidences a negative value of the Poisson ratio ν (elastic constant $C_{12} < 0$), characteristic of an isotropic volume change [54,55]. Since the nontrivial topology is obtained due to d-f band inversion at the X point, SmO is topological as long as the $5d$ band bottom is below the E_{F}. The nontrivial topology is suppressed when the $5d$ band bottom moves above E_{F} or when other bands dip below E_{F} [Fig. 1(b)]. In the case of SmO, it is the $6s$ band bottom

at the Γ point that shifts to lower values as a function of increasing lattice parameter. The shift of the 5*d* and 6*s* band bottoms (at *X* and Γ, respectively) with respect to the E_F as a function of lattice parameter are collected in Fig. 1(d) for the LDA+SO+*U* approach. Treating the strong 4*f* correlations on a mean-field level, the topological semimetal state is quite robust and remains so, up to 5.38 Å , a 9% increase in lattice parameter. On an experimental level, this result is very promising, since it provides a large range of substrate lattice constants for which SmO thin films reveal topological nontriviality. During the evaluation of the topological indices using LDA+SO+*U*, we became aware of another interesting feature, a nontrivial topology due to *s*-*f* band inversion at Γ for 11% and larger lattice constants (⩾5.5Å). In LDA+SO+*U*, the 5*d* band bottom shifts above the E_F and becomes trivial before the 6*s* band bottom dips below E_F. Further increase in the lattice parameter then results in a *s*-*f* band inversion at Γ, which is again topological [Fig. 1(c)]. Albeit no gap will be opened at Γ due to the degenerate quartet in cubic symmetry, thin films of SmO will acquire a tetragonal symmetry induced by strain which lifts the degeneracy and a gap opens, creating a topological insulator. Although the probability for a successful growth of SmO on a substrate with a 11% and larger lattice constant may be low, it nonetheless offers another exciting route towards realizing a topologically nontrivial state, only this time with a *s*-*f* band inversion. We verified the validity of our results for a range of *U* values (5 to 7 eV) and as well as for the MBJLDA exchange potential.

In the calculations so far, we have allowed Sm to be in the intermediate valence state and have treated this on a DFT level. The mixed valent situation can be viewed as a 4*f* to 5*d* promotion of a certain fractional amount of electrons due to the hybridization of the localized 4*f* states with the bandlike 5*d* states. Based on the handful of experimental reports available in literature, the valence assigned to Sm in SmO is 2.92, i.e., a promotion of 0.92 electrons. To actually calculate the amount of electron promotion is a difficult task, since DFT in the Kohn-Sham scheme is based on a single Slater determinant approximation and prevents a correct description of a many-body intermediate valence state. In other words, the position of the 4*f* bands relative to the 5*d*/6*s* as calculated in DFT is not a reliable quantity (see the Appendix). Yet, we can address the effect of mixed valency on the topological properties of SmO in a rigorous quantitative way, by calculating the amount of electrons (integration of the density of states) that can be accommodated in the dispersive 5*d* or 6*s* band, thereby mimicking various amounts of 4*f* $\longrightarrow$ 5*d* or 4*f* $\longrightarrow$ 6*s* promotion. For the lattice constants which has the band inversion at the *X* point, we calculate the amount of electrons that can be contained in the 5*d* band before beginning to populate the 6*s* band. Note that the nontrivial topology is maintained as long as only the 5*d* is occupied *and* the 6*s* remains unoccupied. Figure 3 displays this electron amount as a function of the lattice constant. Analogously, on the other side of the phase diagram, wherein nontriviality is manifested due to a *s*-*f* inversion, we calculate the amount of electrons that can be contained in the 6*s* band before beginning to populate the 5*d* band. Equilibrium lattice constants for the 3+ and 2+ limiting cases are estimated using spin-polarized L(S)DA+SO+*U* schemes. We observe

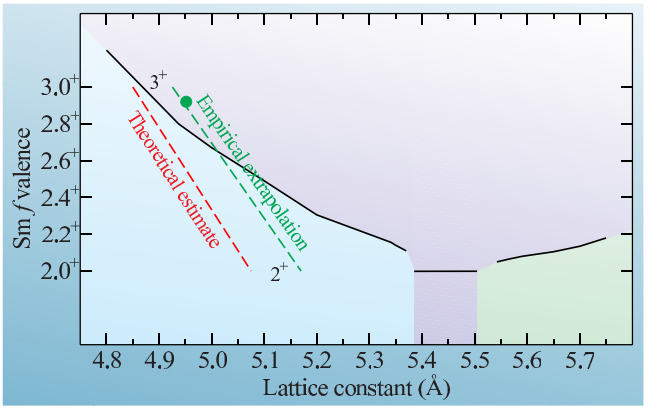

FIG. 3. (Color online) Maximum possible *f* valence due to *f* $\longrightarrow$ *d* or *f* $\longrightarrow$ *s* promotion in SmO while retaining the nontrivial topology as a function of lattice parameter. The color map follows that of Fig. 1(d): light blue = nontrivial topology from *d*-*f* inversion, light green = nontrivial topology from *s*-*f* inversion, light pink = trivial topology. The equilibrium lattice parameters for a high-spin 3+ and 2+ state are computed using the L(S)DA+SO+*U* scheme (dashed red line). The estimates from an empirical extrapolation for the limiting cases are obtained from Ref. [43] (dashed green line). The filled green circle denotes the experimental bulk SmO. SmO remains a topological semimetal for a wide range of tensile strain (⩾1%), since the calculated maximum valence is above both the empirical extrapolation and L(S)DA+U+SO estimates.

that the theoretical estimated valence and lattice constants always yield a topological nontrivial ground state. Though the estimate from an empirical extrapolation for the SmO valence places the bulk in the trivial region of the phase diagram, nontrivial topology is quickly reinstated for lattice parameters with a small tensile strain (⩾1%). Spectroscopy experiments are necessary to confirm the samarium valency, and positions of the samarium *s* and *d* bands with respect to the *f* states in bulk SmO and SmO thin films.

By virtue of the large surface to volume ratio, thin films of systems with nontrivial topology with dominant surface states are highly sought after. Owing to the simple fcc symmetry and the flexibility in observing the topological ground state in SmO for a wide range of lattice parameters, we anticipate plenty of options for suitable substrates. One particular substrate that invokes special interest is the fcc ferromagnetic semiconductor EuO [36–42], which has a lattice constant of 5.14 Å, only a 4% lattice mismatch with that of bulk SmO. EuO by itself is an attractive material with many functionalities, including metal-insulator transition, magnetic phase transition, colossal magnetoresistance, etc. [39–42]. These functionalities have produced an abundance of research on growing high quality thin films of EuO. So, a quick progress in the engineering of SmO/EuO thin film interfaces can be expected. Additionally, this would open up the possibility for another experimental realization of the QAHE, this time in a strongly correlated electron system with topologically nontrivial flat bands. Despite the lack of a bulk band gap in Cr-doped $(Bi,Sb)_2Te_3$ thin films, QAHE was observed at 30 mK [29,30]. In a similar manner, the presence of a semimetallic bulk in SmO will give rise to bulk carriers, but given the tiny electron and hole pockets

around X and Γ, respectively, and by making use of thin films, the amount of bulk charge carriers can be kept quite small and should not completely overshadow the QAHE.

IV. CONCLUSIONS

In summary, we have investigated in detail the electronic structure of SmO and established the nontrivial topology of the band structure such that SmO can be classified as a 3D strongly topological semimetal. The topological state in SmO is very robust and prevails for a wide range of lattice parameters, which leads us to propose SmO as an ideal candidate for further investigations of topologically nontrivial correlated flat bands in bulk and thin-film form.

ACKNOWLEDGMENTS

The authors thank Professor J. Allen, S. Wirth, and P. Thalmeier for discussions. D.K. acknowledges funding by the Deutsche Forschungsgemeinschaft (DFG) within Forschergruppe (FOR) 1346.

APPENDIX

1. Calculation of topological indices

To calculate the $\mathbb{Z}_2$ topological index for a system with inversion symmetry, we use the parity criteria as proposed by Fu and Kane [3], wherein the product of the parities of all occupied Kramers doublets at each time reversal invariant momentum (TRIM) is determined. For an fcc lattice, and hence a bcc Brillouin zone, we have the following eight TRIM points: one Γ (0,0,0), three X $(1,0,0)2\pi/a$, and four L $(\frac{1}{2},\frac{1}{2},\frac{1}{2})2\pi/a$. The sign of the product of the parities of all occupied doublets (Kramers degenerate bands) at these eight TRIM points refer to a trivial topology when positive and to a nontrivial topology when negative. Under spatial inversion, the d orbitals are even while the f orbitals are odd. From the calculated band structures, it is clear that the occupied bands between 0 and -2 eV at Γ and the four L points possess f orbital character, while due to the $4f$-$5d$ band inversion, one of the occupied band at the three X points possesses d orbital character. The product of the parities for all the occupied bands will then be negative, giving rise to a nontrivial topology in the band structure of SmO. This result is valid for both LDA+SO and LDA+SO+U calculations. This qualitative discussion was confirmed by explicitly calculating the space group representations of the inversion operator of all bands at the TRIM points (Table I). This gives access to the four topological indices $\nu_0;(\nu_1\nu_2\nu_3)$. The resulting indices for all bands up to the highest occupied $4f_{5/2}$ bands are $1;(000)$, which makes SmO strongly topological. As a result of the particular arrangement of the bands around the E_F in SmO, which creates a semimetallic "warped gap" (no band crossings at E_F), it is possible to apply the parity counting scheme at the TRIM points, since this warped gap ensures the continuity condition for the phases of the wave functions in the whole BZ, which leads to the counting scheme. In consequence one could classify SmO as a 3D strongly topological semimetal.

The topological indices switch from trivial to nontrivial at the bottom of the six $4f_{5/2}$ derived bands and switch back to trivial above the band, which forms the electron pockets around the X point, which in consequence tells us that topological surface bands could bridge the energy window from the lowest $4f_{5/2}$ band to the lowest unoccupied $5d$ band. In Table I we provide the details of the topological character of the important bands. The energy separation of about 2 eV between the O $2p$ bands and the lowest $4f$ state ensures that the gap between O $2p$ and Sm $4f$ must be trivial due to the fact that SO coupling is too small to create band inversions bridging this gap. Hence the highest O $2p$ band forms the trivial base line for discussing the topological properties of the remaining bands. In the table we list the energy of the bands at the Γ point, the band indices (as indicated in Fig. 4), the parity of the Kramers doublets

TABLE I. Calculated topological indices of selected bands in SmO within LDA+SO+U approximation ($a = 4.941$ Å). ε_n refers of the band energy at Γ and n refers to the band indices, shown in Fig. 4. Γ, X, and L are the TRIM points. $\nu_0;(\nu_1\nu_2\nu_3)$ are the four topological indices. The parity of the Kramers doublet at the various TRIM points are denoted by O (odd) and E (even). Additionally, the dominating orbital character of the bands at the TRIM points are listed.

$\varepsilon_n(\Gamma)$ eV, (n)	Γ	$3\times X$	$4\times L$	$\nu_0;(\nu_1\nu_2\nu_3)$
-3.650	O $(2p)$	O $(2p)$	E $(2p)$	$0;(000)$
-0.493 (1,2)	O $(4f_{5/2})$	E $(5d)$	O $(4f_{5/2})$	$1;(000)$
$+0.030$ (3,4)	O $(4f_{5/2})$	O $(4f_{5/2})$	O $(4f_{5/2})$	$1;(000)$
$+0.030$ (5,6)	O $(4f_{5/2})$	O $(4f_{5/2})$	O $(4f_{5/2})$	$1;(000)$
$+1.457$ (7,8)	E $(6s)$	O $(5d)$	E $(5d)$	$0;(000)$

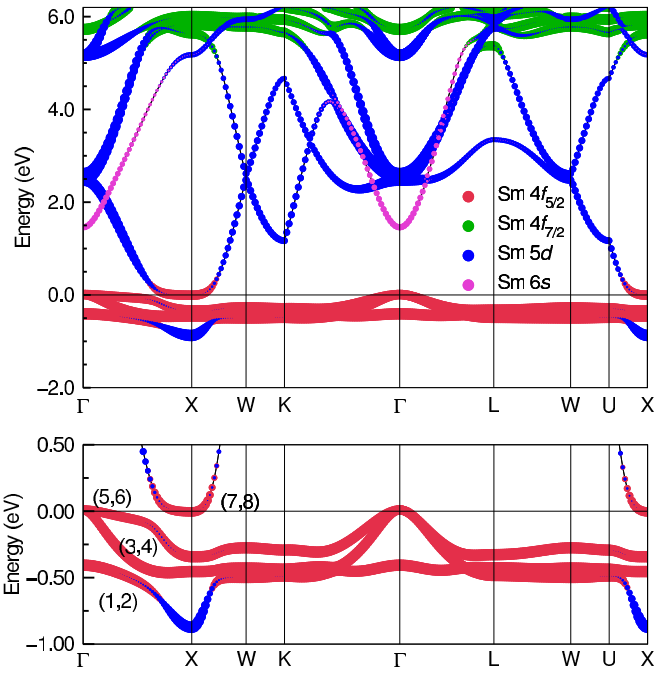

FIG. 4. (Color online) The calculated FPLO band structure of SmO ($a = 4.941$Å) within a nonspin polarized, full-relativistic approximation including strong Coulomb correlation (LDA+SO+U). A U and J_H value of 6 and 0 eV have been used, respectively. The size of the symbols represent the weight of the various orbital contributions to the underlying bands. The numbers within parentheses are band indices to assist in assigning the various topological indices in Table I.

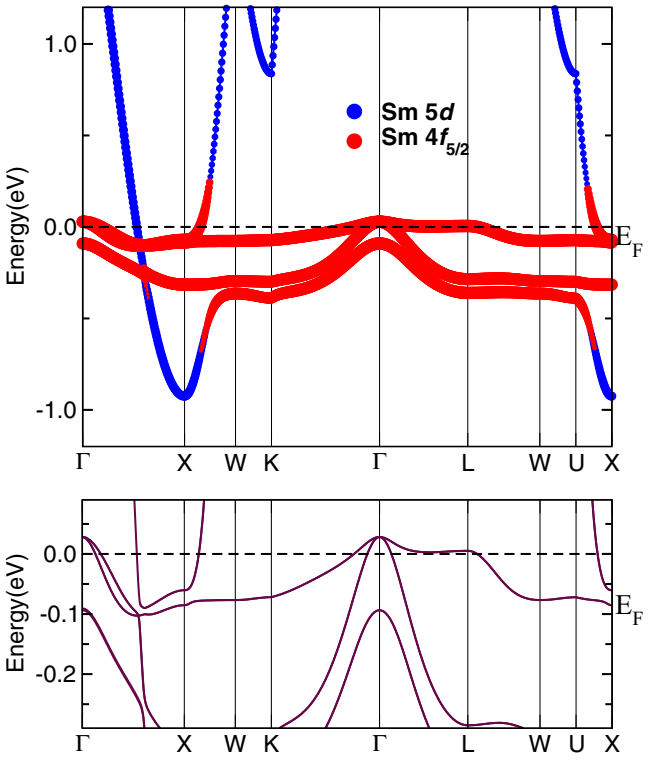

FIG. 5. (Color online) Band structure of SmO with orbital character using MBJLDA+SO approximation as implemented in WIEN2K. The topology and order of the bands are consistent to the ones obtained using the LDA+SO+U scheme. The blow-up in the bottom panel clearly shows the opening of the warped band gap along Γ-X, but smaller in size compared to FPLO. For clarity we have plotted the bands without any band character.

(O: odd, E: even) together with the dominating orbital character at the three symmetry distinguished classes of TRIM points, as well as the resulting topological indices obtained from all bands including the ones mentioned in the first column. Note that, bands numbered 3 to 6 are trivial bands, and do not change the topology.

2. Band structure using modified Becke-Johnson approach

To make sure that the topological characteristics are not dependent on the choice of exchange and correlation functional, we calculated the band structure of SmO using the recently proposed modified Becke-Johnson functional (MBJLDA) as implemented in WIEN2K. Figure 5 shows the band structure obtained using MBJLDA+SO. The f-d band inversion at X point is consistent with our LDA+SO+U calculations, though the hybridization gap and the warped band gap in MBJLDA+SO are smaller (but of the same order).

3. Surface state calculations

To assess the nature of the surface band structure we calculated the Bloch spectral density [$A_{\rm Bl}(k)$] of the 12 topmost surface layers of a semi-infinite solid with [001] surface. For this purpose the DFT band structure was fitted with atom centered maximally projected Wannier functions of Sm 5d, 6s, and 4f and O 2p character. A soft energy cutoff was employed to achieve band disentanglement at +6 eV. The resulting fit models all relevant bands around the Fermi level within a few meV accuracy. Afterwards, the obtained bulk hopping parameters were mapped onto a semi-infinite solid and a Green's function technique was used to calculate $A_{\rm Bl}(k)$ for the surface layers. The resulting surface bands clearly show two weakly interacting Dirac cones around the surface projected $\bar{M}$ point. In order to be of topology induced nature, there must be an odd number of Dirac cones. The surface Brillouin zone for a [001] surface ends up with two bulk X points being projected onto the surface $\bar{M}$ point and one bulk X point being projected onto the surface $\bar{\Gamma}$ point (see Fig. 6). Hence, one expects two Dirac cones at $\bar{M}$ and one at $\bar{\Gamma}$. The backfolding of the bulk band structure due to projection onto [001] leads to the appearance of electron pocket states from the bulk X point at $\bar{\Gamma}$, which overlap with the bulk projected states of the bulk Γ hole pocket at $\bar{\Gamma}$. Hence, the third Dirac cone will be immersed into projected bulk states and can only form a surface resonance. In order to prove the existence of this third Dirac cone, we performed an additional calculation, where the 4f electron pocket around the bulk Γ point are lowered in energy by application of a **k**-dependent potential. This removes bulk projected states from the low energy region at the surface $\bar{\Gamma}$ point and reveals the third Dirac cone. Finally, to rule out drastic effects of the relaxation of the surface electronic structure we performed a full DFT slab calculation for 21 SmO layers. The resulting slab band structure shows the same two weakly interacting Dirac cones around the $\bar{M}$ point as the semi-infinite calculation. Slight shifts of bands occur, but the overall structure equals that of the mapped model calculation.

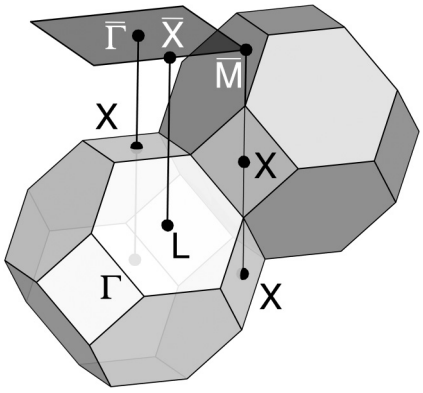

FIG. 6. Bulk and surface Brillouin zone of an fcc lattice.

4. Notes on the many-body state of SmO

The Sm 4f states are known to be strongly correlated. Nonetheless, one can obtain useful information about this system using DFT within the local density approximation. The large on-site Coulomb repulsion between the f electrons restricts the local valence occupations to fluctuate between the f^5 and f^6 configurations. The lattice constants for the limiting cases of a pure 2+ (f^6) and pure 3 + (f^5) SmO compound are determined using spin polarized L(S)DA+SO+U. The local atomic f^6 (f^5) configuration has a lowest Hunds-rule

multiplet state which belongs to the ${}^7F({}^6H)$ term. LDA in the Kohn-Sham scheme does capture these local states as they are single Slater determinant representable (as any Hunds-rule high spin ground state).

In order to determine the topology of the bands and in order to answer the question if hybridization between the Sm d derived bands and the Sm f derived bands is allowed, it is important to have the local symmetry correct. The spin polarized state found in L(S)DA does not represent the local Sm f^6 character correctly. Within L(S)DA the Sm f^6 configuration has a local moment ($M_z = 2S_z + Lz = 3$), whereas the many-body ground state is a singlet [$\langle J^2\rangle = J(J+1) = 0$] without a local moment ($L_z = 0$, $S_z = 0$, $M_z = 0$). The many-body ground state without a local moment is consistent with experimental observations on divalent Sm compounds. In order to reproduce the local symmetry of the many-body state of an f^6 configuration (${}^7F_0$ term with $J = 0$, belonging to the A_{1g} representation) we use nonspin polarized DFT calculations. In this case the f^6 configuration is represented by a state with six electrons in the $j = 5/2$ bands. Although this state has an incorrect expectation value of L ($\langle L^2\rangle = 24/7$) and S ($\langle S^2\rangle = 24/7$) compared to the many-body state (and thus a to high local Coulomb energy), it does have the right symmetry (A_{1g}) and total momentum ($J = 0$). The f^5 configuration is represented by single hole excitations starting from the f^6 configuration. A peculiarity of starting from a many-body f^6 state with A_{1g} symmetry is that the many-body one electron excitations have the same symmetry as the independent electron bands found in LDA, as shown by Martin and Allen [51].

[1] C. L. Kane and E. J. Mele, Phys. Rev. Lett. **95**, 146802 (2005).
[2] C. L. Kane and E. J. Mele, Phys. Rev. Lett. **95**, 226801 (2005).
[3] L. Fu and C. L. Kane, Phys. Rev. B **76**, 045302 (2007).
[4] J. E. Moore and L. Balents, Phys. Rev. B **75**, 121306(R) (2007).
[5] R. Roy, Phys. Rev. B **79**, 195321 (2009).
[6] L. Fu, C. L. Kane, and E. J. Mele, Phys. Rev. Lett. **98**, 106803 (2007).
[7] H. Zhang, C.-X. Liu, X.-L. Qi, X. Dai, Z. Fang, and S.-C. Zhang, Nat. Phys. **5**, 438 (2009).
[8] M. Konig, S. Wiedmann, C. Brune, A. Roth, H. Buhmann, L. W. Molenkamp, X. L. Qi, and S. C. Zhang, Science **318**, 766 (2007).
[9] D. Hsieh, D. Qian, L. Wray, Y. Xia, Y. S. Hor, R. J. Cava, and M. Z. Hasan, Nature (London) **452**, 970 (2008).
[10] D. Hsieh, Y. Xia, L. Wray, D. Qian, A. Pal, H. Dil, J. Osterwalder, F. Meier, G. Bihlmayer, C. L. Kane, Y. S. Hor, R. J. Cava, and M. Z. Hasan, Science **323**, 919 (2009).
[11] Y. Xia, D. Qian, D. Hsieh, L. Wray, A. Pal, H. Lin, A. Bansil, D. Grauer, Y. S. Hor, R. J. Cava, and M. Z. Hasan, Nat. Phys. **5**, 398 (2009).
[12] Y. L. Chen, J. G. Analytis, J.-H. Chu, Z. K. Liu, S.-K. Mo, X. L. Qi, H. J. Zhang, D. H. Lu, X. Dai, Z. Fang, S. C. Zhang, I. R. Fisher, Z. Hussain, and Z.-X. Shen, Science **325**, 325 (2009).
[13] E. Bergholtz and Z. Liu, Int. J. Mod. Phys. B **27**, 1330017 (2013).
[14] Z. Liu, E. J. Bergholtz, and E. Kapit, Phys. Rev. B **88**, 205101 (2013).
[15] S. Flach, D. Leykam, J. D. Bodyfelt, P. Matthies, and A. S. Desyatnikov, Europhys. Lett. **105**, 30001 (2014).
[16] S. Kourtis, T. Neupert, C. Chamon, and C. Mudry, Phys. Rev. Lett. **112**, 126806 (2014).
[17] A. G. Grushin, Á. Gómez-León, and T. Neupert, Phys. Rev. Lett. **112**, 156801 (2014).
[18] M. Dzero, K. Sun, V. Galitski, and P. Coleman, Phys. Rev. Lett. **104**, 106408 (2010).
[19] M. Dzero, K. Sun, P. Coleman, and V. Galitski, Phys. Rev. B **85**, 045130 (2012).
[20] T. Takimoto, J. Phys. Soc. Jpn. **80**, 123710 (2011).
[21] S. Wolgast, Ç. Kurdak, K. Sun, J. W. Allen, D.-J. Kim, and Z. Fisk, Phys. Rev. B **88**, 180405(R) (2013).
[22] D. J. Kim, J. Xia, and Z. Fisk, Nat. Mater. **13**, 466 (2014).
[23] S. Suga, K. Sakamoto, T. Okuda, K. Miyamoto, K. Kuroda, A. Sekiyama, J. Yamagichi, H. Fujiwara, A. Irizawa, T. Ito, S. Kimura, T. Balashov, W. Wulfhekel, S. Yeo, F. Iga, and S. Imada, J. Phys. Soc. Jpn. **83**, 014705 (2014).
[24] Z.-H. Zhu, A. Nicolaou, G. Levy, N. P. Butch, P. Syers, X. F. Wang, J. Paglione, G. A. Sawatzky, I. S. Elfimov, and A. Damascelli, Phys. Rev. Lett. **111**, 216402 (2013).
[25] Z. Li, J. Li, P. Blaha, and N. Kioussis, Phys. Rev. B **89**, 121117(R) (2014).
[26] J. Herber, Nature (London) **459**, 28 (2009).
[27] J. Mannhart and D. G. Schlom, Science **327**, 1607 (2010).
[28] H. Ji, J. M. Allred, N. Ni, J. Tao, M. Neupane, A. Wray, S. Xu, M. Z. Hasan, and R. J. Cava, Phys. Rev. B **85**, 165313 (2012).
[29] C. Chang, J. Zhang, X. Feng, J. Shen, Z. Zhang, M. Guo, K. Li, Y. Ou, P. Wei, L. Wang, Z. Ji, Y. Feng, S. Ji, X. Chen, J. Jia, X. Dai, Z. Fang, S. Zhang, K. He, Y. Wang, L. Lu, X. Ma, and Q. Xue, Science **340**, 167 (2013).
[30] H. Ke, M. Xu-Cun, C. Xi, L. Li, W. Ya-Yu, and X. Qi-Kun, Chin. Phys. B **22**, 067305 (2013).
[31] L. Fu and C. L. Kane, Phys. Rev. Lett. **102**, 216403 (2009).
[32] A. R. Akhmerov, J. Nilsson, and C. W. J. Beenakker, Phys. Rev. Lett. **102**, 216404 (2009).
[33] A. M. Cook and A. Paramekanti, Phys. Rev. Lett. **113**, 077203 (2014).
[34] T. Cai, X. Li, F. Wang, J. Sheng, J. Feng, and C. Gong, arXiv:1310.2471.
[35] K. F. Garrity and D. Vanderbilt, Phys. Rev. Lett. **110**, 116802 (2013).
[36] B. T. Matthias, R. M. Bozorth, and J. H. Van Vleck, Phys. Rev. Lett. **7**, 160 (1961).
[37] W. Nolting, Phys. Status Solidi B **96**, 11 (1979).
[38] G. Adachi and N. Imanaka, Chem. Rev. **98**, 1479 (1998).
[39] P. G. Steeneken, L. H. Tjeng, I. Elfimov, G. A. Sawatzky, G. Ghiringhelli, N. B. Brookes, and D. J. Huang, Phys. Rev. Lett. **88**, 047201 (2002).
[40] A. Schmel, V. Vaithyanathan, A. Herrnberger, S. Thiel, C. Richter, M. Liberati, T. Heeg, M. Röckerath, L. Kourkoutis, S. Mühlbauer, P. Böni, D. A. Muller, Y. Barash, J. Schubert, Y. Idzerda, J. Mannhart, and D. Schlom, Nat. Mater. **6**, 882 (2007).

[41] R. Sutarto, S. G. Altendorf, B. Coloru, M. Moretti Sala, T. Haupricht, C. F. Chang, Z. Hu, C. Schüßler-Langeheine, N. Hollmann, H. Kierspel, H. H. Hsieh, H. J. Lin, C. T. Chen, and L. H. Tjeng, Phys. Rev. B **79**, 205318 (2009).
[42] A. Melville, T. Mairoser, A. Schmehl, M. Fischer, S. Gsell, M. Schreck, D. D. Awschalom, T. Heeg, B. Holländer, J. Schubert, and D. G. Schlom, App. Phys. Lett. **103**, 222402 (2013).
[43] J. M. Leger, N. Yacoubi, and J. Loriers, Inorg. Chem. **19**, 2252 (1980).
[44] G. Krill, M. F. Ravet, J. P. Kappler, L. Abadli, J. M. Leger, N. Yacoubi, and C. Loriers, Solid State Commun. **33**, 351 (1980).
[45] J. M. Leger, P. Almonino, J. Loriers, P. Dordor, and B. Coqblin, Phys. Lett. A **80**, 325 (1980).
[46] K. Koepernik and H. Eschrig, Phys. Rev. B **59**, 1743 (1999).
[47] J. P. Perdew and Y. Wang, Phys. Rev. B **45**, 13244 (1992).
[48] M. T. Czyżyk and G. A. Sawatzky, Phys. Rev. B **49**, 14211 (1994).
[49] F. Tran and P. Blaha, Phys. Rev. Lett. **102**, 226401 (2009).
[50] P. Blaha and K. Schwarz, Comput. Mater. Sci. **28**, 259 (2003).
[51] R. Martin and J. Allen, J. Appl. Phys. **50**, 7561 (1979).
[52] H. Zhang and S.-C. Zhang, Phys. Status Solidi RRL **7**, 72 (2013).
[53] J. Velev and W. Butler, J. Phys. Condens. Matter **16**, R637 (2004).
[54] B. Lüthi, J. Magn. Magn. Mater. **52**, 70 (1985).
[55] P. Wachter, *Handbook on the Physics and Chemistry of Rare Earths* (North-Holland, Amsterdam, 1998), Vol. 19, Chap. 132.